Vietnam Journal of Mechanics, Vol. 46, No. 2 (2024), pp. 119 – 137
DOI: https://doi.org/10.15625/0866-7136/20702

SIZE-DEPENDENT NONLINEAR BENDING OF MICROBEAMS BASED ON A THIRD-ORDER SHEAR DEFORMATION THEORY

Ngoc Duyen Dang[1,2], **Dinh Kien Nguyen**[2,3], **Cong Ich Le**[4,*]
[1]*Faculty of Mechanical Engineering, Thuyloi University, 175 Tay Son, Dong Da, Hanoi, Vietnam*
[2]*Graduate University of Science and Technology, VAST, 18 Hoang Quoc Viet, Hanoi, Vietnam*
[3]*Institute of Mechanics, VAST, 18 Hoang Quoc Viet, Hanoi, Vietnam*
[4]*Faculty of Mechanical Engineering, Le Quy Don Technical University, 236 Hoang Quoc Viet, Hanoi, Vietnam*
[*]E-mail: lecongich79@lqdtu.edu.vn

Received: 01 May 2024 / Revised: 22 May 2024 / Accepted: 03 June 2024
Published online: 10 June 2024

Abstract. In this paper, the size-dependent nonlinear bending of microbeams subjected to mechanical loading is studied using a finite element formulation. Based on the von Kármán nonlinear relationship and the third-order shear deformation theory, a size-dependent nonlinear beam element is derived by using the modified couple stress theory (MCST) to capture the microstructural size effect. The element with explicit expressions for the element vector of internal forces and tangent stiffness matrix is derived by employing the transverse shear rotation as a variable. Nonlinear bending of microbeams under different mechanical loading is predicted with the aid of Newton–Raphson iterative method. Numerical investigation shows that the derived element is efficient, and it is capable of giving accurate results by several elements. The obtained results reveal the importance of the micro-size effect on the nonlinear behavior of the microbeams, and the deflections are overestimated when the microstructural effect is ignored. The effects of the material length scale parameter, boundary conditions and loading type on the bending response of the microbeams are studied and highlighted.

Keywords: microbeam, micro-size effect, nonlinear bending, finite element formulation.

1. INTRODUCTION

Microbeams are used in many small-scale systems and devices such as micro/nano-electro-mechanical systems (MEMS/NEMS) [1]. Due to complex loading, microbeams in such application are often undergone large deformation. Understanding large deformation of micro-scale structural elements is important for proper use and design of the microdevices and microsystem, and this motivates investigations on nonlinear bending behaviour of microstructure in general, and microbeams in particular. Regarding the nonlinear bending of microbeams, many efforts have been made to predict response of microbeams under different electronic and/or mechanical loading. In the early works, the classical beam theories, which are unable to describe the influence of the size effects, have been employed to model the microbeams [2–5]. In these works, the von Kármán nonlinear assumption is adopted to account for the relatively large rotation, and the response of the microbeams is assessed by various methods, e.g the shooting method [2], the Galerkin method [3,4].

To amend the shortcomings of the classical theories in modeling the size effects in small-scale structures, various higher-order continuum theories such as the strain gradient elasticity theory (SGET) [5,6], the modified couple stress theory (MCST) [7], which contain the length scale parameters, have been proposed. Using these higher-order continuum theories, investigations on the influence of micro-size effect on mechanical behavior of microbeams and microframes have been carried out in recent years. For instance, Mohammadi and Mahzoon [8] derived the governing equations for postbuckling analysis of Euler-Bernoulli microbeams, in which both SGET and MCST have been employed to model the microsize effects. By introducing a material length scale parameter in a new nonlinear beam model, Xia et al. [9] presented the size-dependent analyses of static bending, post-critical, and vibration of microbeams. Asghari et al. [10] proposed a Timoshenko microbeam model for nonlinear vibration and bending analyses of micro-scale beams, in which the size effects are captured through the MCST and SGET. The SGET was used in conjunction with Timoshenko beam theory by Ramezani [11] to study vibration of microbeams with large amplitude, showing the importance of geometric nonlinearity in enhancement of the beam frequencies. Buckling behavior of functionally graded (FG) microbeams with different boundary conditions was investigated by Akgoz and Civalek [12] in the framework of Euler–Bernoulli beam theory and the modified strain gradient theory. Euler–Bernoulli beam theory was used in conjunction with MCST by Wang et al. [13] to study nonlinear bending and thermal post-buckling of microbeams, considering the effect of Poisson's ratio. The shooting method was used in combination with Newton iterative method in the work to determine the deflections and post-critical paths of the microbeams. The MCST was employed with differential quadrature method (DQM) by Ansari et al. [14] to study bending, stability and vibration of nonlinear FG

microbeams. The parametric study focused on the dependence of frequencies and critical loads upon the thickness-to-material length scale ratio. Additionally, Dadgar-Rad and Beheshti [15] explored the large deformation of microframes by a total Lagrange element, while Attia and Mohamed [16] considered thermal instability of FG microbeams using the DQM. Their finding reveals the importance of microstructural effect on the thermal stability and bending of the microbeams.

The size-dependent nonlinear bending of micro-scale beams is studied in the present work by using a finite element formulation. Based on the third-order shear deformation theory and MCST, a nonlinear beam element is derived and used to establish equilibrium equation. The element based on von Kármán nonlinear assumption is formulated by using transverse shear rotation, not cross-sectional rotation, as a variable to ensure an quadratic variation of moment along the beam length. Nonlinear response of microbeams with various boundary conditions under different distributed loads is predicted with the aid of the Newton–Raphson iterative method. The influence of the material length scale parameter, the boundary conditions and the loading type on nonlinear behavior of the microbeams is studied in detail and highlighted.

2. MATHEMATICAL FORMULATION

An isotropic microbeam, with length L, width b, and thickness h under mechanical loading is considered. A Cartesian coordinate system (x, y, z) is introduced as well as the x-axis directs along the beam axis; y- and z-axes are coincident with the principal axes of the root cross-section. According to the third-order shear deformation theory [17], the displacements of a point inside the microbeam are given by

$$\begin{aligned} u(x,z) &= u_0(x) + z\theta(x) - \frac{4z^3}{3h^2}\left[\theta(x) + w_{0,x}(x)\right], \\ w(x,z) &= w_0(x), \end{aligned} \tag{1}$$

in which $u_0(x)$ and $w_0(x)$ are displacements in the x and z directions of a point on x-axis, respectively; $\theta(x)$ is the cross-sectional rotation. In Eq. (1) and hereafter, a subscript comma indicates the partial derivative with respect to the followed variable, e.g. $w_{0,x} = \partial w_0/\partial x$.

Since a beam element based on the cross-sectional rotation $\theta(x)$ and linear interpolation for $u_0(x)$ and $\theta(x)$ is poor convergent due to not satisfy a quadratic variation of moment along the length, Shi and Lam [18] proposed to use the following transverse shear rotation as an independent variable

$$\gamma_0(x) = \theta(x) + w_{0,x}(x). \tag{2}$$

Using the transverse shear rotation γ_0, one can recast the displacements in Eq. (1) in the following forms

$$\begin{aligned} u(x,z) &= u_0 - z\,(w_{0,x} - \gamma_0) - \frac{4z^3}{3h^2}\gamma_0, \\ w(x,z) &= w_0. \end{aligned} \tag{3}$$

It is noted that the x variable is dropped from the quantities in the above equation and below for the sake of simplicity.

Based on the von Kármán nonlinear assumption, the normal and shear strains deduced from Eq. (3) are

$$\begin{aligned} \varepsilon_{xx} &= u_{,x} + \frac{1}{2}w_{,x}^2 = \varepsilon_0 - z\,(w_{0,xx} - \gamma_{0,x}) - \frac{4z^3}{3h^2}\gamma_{0,x}, \\ \gamma_{xz} &= u_{,z} + w_{,x} = \gamma_0\Big(1 - \frac{4z^2}{h^2}\Big), \end{aligned} \tag{4}$$

where $\varepsilon_0 = u_{0,x} + \dfrac{1}{2}w_{0,x}^2$ is the membrane strain.

Assuming Hook's law for the material, the normal stress σ_{xx} and the shear stress τ_{xz} are related to the associated strains according to

$$\left\{ \begin{array}{c} \sigma_{xx} \\ \tau_{xz} \end{array} \right\} = \left[\begin{array}{cc} E & 0 \\ 0 & G \end{array} \right] \left\{ \begin{array}{c} \varepsilon_{xx} \\ \gamma_{xz} \end{array} \right\}, \tag{5}$$

where E and $G = \dfrac{E}{2(1+\nu)}$ are the Young's modulus and shear modulus, respectively.

Since the classical beam theory is not able to describe the microstructural size effect, the MCST [7] is adopted in conjunction with the above third-order shear deformation beam theory herein to evaluate the strain energy of the microbeam as

$$\mathcal{U} = \frac{1}{2}\int_V (\boldsymbol{\sigma} : \boldsymbol{\varepsilon} + \boldsymbol{m} : \boldsymbol{\chi},)\mathrm{d}V, \tag{6}$$

where V is the microbeam volume; $\boldsymbol{\sigma}$ and $\boldsymbol{\varepsilon}$ are, respectively, the stress and strain tensors; $\boldsymbol{m}$ is the deviatoric part of the couple stress tensor and $\boldsymbol{\chi}$ is the symmetric curvature tensor. The expressions for theses tensors are as follows [7]

$$\begin{aligned} &\boldsymbol{\sigma} = \alpha\ \mathrm{tr}(\boldsymbol{\varepsilon})\boldsymbol{I} + 2G\boldsymbol{\varepsilon}, \ \ \boldsymbol{\varepsilon} = \frac{1}{2}[\nabla\boldsymbol{u} + (\nabla\boldsymbol{u})^T], \\ &\boldsymbol{\chi} = \frac{1}{2}[\nabla\boldsymbol{\beta} + (\nabla\boldsymbol{\beta})^T], \ \ \boldsymbol{m} = 2\ell^2 G\boldsymbol{\chi}, \end{aligned} \tag{7}$$

with α and G are Láme's constants (G, as mentioned above, is also the shear modulus); ℓ is the material length scale parameter; $\boldsymbol{\beta}$ and $\boldsymbol{u}$ are, respectively, the rotation vector and

the displacement vector, that can be expressed as

$$\boldsymbol{\beta} = \frac{1}{2}\mathrm{curl}(\boldsymbol{u}), \quad \boldsymbol{u} = \{u,\ 0,\ w\}^T. \tag{8}$$

The strain energy in Eq. (6) can now be written in the form

$$\mathcal{U} = \frac{1}{2}\int_0^L \int_A (\sigma_{xx}\varepsilon_{xx} + \tau_{xz}\gamma_{xz} + 2m_{xy}\chi_{xy} + 2m_{yz}\chi_{yz})\mathrm{d}A\mathrm{d}x, \tag{9}$$

where $A = b \times h$ is cross-section area, and

$$\begin{aligned} \chi_{xy} &= -\frac{1}{2}w_{0,xx} + \frac{1}{4}\gamma_{0,x} - \frac{z^2}{h^2}\gamma_{0,x}, \quad m_{xy} = 2G\ell^2\chi_{xy}, \\ \chi_{yz} &= -\frac{2z}{h^2}\gamma_0, \quad m_{yz} = 2G\ell^2\chi_{yz}. \end{aligned} \tag{10}$$

From Eqs. (4), (5) and (10), one can recast (9) in the form

$$\begin{aligned} \mathcal{U} = \frac{1}{2}\int_0^L \Big\{ & EA\varepsilon_0^2 + EI\Big(w_{0,xx}^2 - \frac{8}{5}w_{0,xx}\gamma_{0,x} + \frac{68}{105}\gamma_{0,x}^2\Big) + \frac{8}{15}GA\gamma_0^2 \\ & + GA\ell^2\Big(w_{0,xx}^2 - \frac{2}{3}w_{0,xx}\gamma_{0,x} + \frac{2}{15}\gamma_{0,x}^2 + \frac{4}{3h^2}\gamma_0^2\Big)\Big\}\,\mathrm{d}x, \end{aligned} \tag{11}$$

where $I = bh^3/12$ is the moment of inertia of cross-section.

The work of external loads is given by

$$\mathcal{W}_{ex} = \int_0^L w(x)q(x)\mathrm{d}x \ + \ \sum_{i=1}^{n_Q} Q_i(x)w(x_i), \tag{12}$$

where $q(x)$ is the distributed load along the length of the microbeam; $Q_i(x_i)$ are the concentrated loads at point x_i; n_Q is the number of the concentrated loads applied to the beam.

The nonlinear equilibrium equation system for the microbeam can be obtained from the principle of virtual work, which can be written as

$$\delta\mathcal{U} - \delta\mathcal{W}_{ex} = 0. \tag{13}$$

Eq. (13) results in a system of nonlinear differential equations with three unknowns u_0, w_0 and γ_0. However, it is very difficult to solve the equations by an analytical method. The finite element method, an effective tool for handling nonlinear problems, is adopted herein instead of.

3. SOLUTION METHOD

This section formulates a two-node beam element. The element vector of degrees of freedom, ($\boldsymbol{\Delta}_e$), contains the displacements and shear rotation at the two nodes as

$$\boldsymbol{\Delta}_e = \{\boldsymbol{u}_0,\ \boldsymbol{w}_0,\ \boldsymbol{\gamma}_0\}^T, \tag{14}$$

in which

$$\boldsymbol{u}_0 = \{u_{0_1},\ u_{0_2}\}^T,\ \boldsymbol{w}_0 = \{w_{0_1},\ w_{0_1x},\ w_{0_2},\ w_{0_2x}\}^T,\ \boldsymbol{\gamma}_0 = \{\gamma_{0_1},\ \gamma_{0_2}\}^T, \tag{15}$$

are the vectors of nodal displacements in x and z directions, and the nodal shear rotations, respectively.

The interpolations for the displacement field are as follows [18]

$$u_0 = \mathbf{h}\,\boldsymbol{u}_0,\ \ w_0 = \mathbf{h}_w\boldsymbol{w}_0,\ \ \gamma_0 = \mathbf{h}\,\boldsymbol{\gamma}_0, \tag{16}$$

where $\mathbf{h}$ is the matrix of linear functions, and $\mathbf{h}_w$ is the matrix of cubic polynomials, and they have the following forms [19]

$$\begin{aligned} \mathbf{h} &= \left\{1 - \frac{x}{l_e},\ \frac{x}{l_e}\right\}, \\ \mathbf{h}_w &= \left\{1 - \frac{3x^2}{l_e^2} + \frac{2x^3}{l_e^3},\ x - \frac{2x^2}{l_e} + \frac{x^3}{l_e^2},\ \frac{3x^2}{l_e^2} - \frac{2x^3}{l_e^3},\ -\frac{x^2}{l_e} + \frac{x^3}{l_e^2}\right\}. \end{aligned} \tag{17}$$

From Eq. (16), one can compute

$$u_{0,x} = \mathbf{b}\boldsymbol{u}_0\,,\ w_{0,x} = \mathbf{b}_w\,\boldsymbol{w}_0\,,\ \gamma_{0,x} = \mathbf{b}\,\boldsymbol{\gamma}_0\,,\ w_{0,xx} = \mathbf{c}_w\,\boldsymbol{w}_0, \tag{18}$$

where

$$\mathbf{b} = \mathbf{h}_{,x},\ \ \mathbf{b}_w = \mathbf{h}_{w,x},\ \ \mathbf{c}_w = \mathbf{h}_{w,xx}. \tag{19}$$

The axial strain as given by Eq. (4) and the interpolating functions (17), (18), (19) cannot be used directly to generate a finite element formulation due to the membrane locking effect. In order to avoid this problem, the membrane strain ε_0 in Eq. (4) is replaced by an effective strain defined as [20]

$$\varepsilon_{\text{eff.}} = \frac{1}{l_e}\int_0^{l_e} \varepsilon_0 \mathrm{d}x = \frac{1}{l_e}\int_0^{l_e}\left(u_{0,x} + \frac{1}{2}w_{0,x}^2\right)\mathrm{d}x. \tag{20}$$

Using Eqs. (17), (18) and (19), one can write Eq. (20) in the form

$$\varepsilon_{\text{eff.}} = \mathbf{b}\boldsymbol{u}_0 + \boldsymbol{w}_0^T\mathbf{B}\,\boldsymbol{w}_0, \tag{21}$$

with

$$\mathbf{B} = \frac{1}{2l_e}\int_0^{l_e} \mathbf{b}_w \mathbf{b}_w^T \mathrm{d}x = \frac{1}{60l_e^2}\begin{bmatrix} 36 & 3l_e & -36 & 3l_e \\ 3l_e & 4l_e^2 & -3l_e & -l_e^2 \\ -36 & -3l_e & 36 & -3l_e \\ 3l_e & -l_e^2 & -3l_e & 4l_e^2 \end{bmatrix}. \tag{22}$$

With the interpolations, the strain energy in Eq. (11) can be written in a matrix form as

$$\begin{aligned} \mathcal{U} = \sum^{\mathrm{NE}} \mathcal{U}^e = \frac{1}{2}\sum^{\mathrm{NE}} \Big\{ & EA\, l_e \Big(\mathbf{b}\boldsymbol{u}_0 + \boldsymbol{w}_0^T \mathbf{B}\, \boldsymbol{w}_0\Big)^2 + \frac{8}{15} GA(\boldsymbol{\gamma}_0^T \mathbf{H}\, \boldsymbol{\gamma}_0) \\ & + EI\Big((\boldsymbol{w}_0^T \mathbf{C}\, \boldsymbol{w}_0) - \frac{8}{5}(\mathbf{c}\, \boldsymbol{w}_0)(\mathbf{b}\, \boldsymbol{\gamma}_0) + \frac{68\, l_e}{105}(\mathbf{b}\, \boldsymbol{\gamma}_0)^2\Big) \\ & + GA\ell^2\Big((\boldsymbol{w}_0^T \mathbf{C}\, \boldsymbol{w}_0) - \frac{2}{3}(\mathbf{c}\, \boldsymbol{w}_0)(\mathbf{b}\, \boldsymbol{\gamma}_0) + \frac{2\, l_e}{15}(\mathbf{b}\, \boldsymbol{\gamma}_0)^2 + \frac{4}{3h^2}(\boldsymbol{\gamma}_0^T \mathbf{H}\, \boldsymbol{\gamma}_0)\Big)\Big\}, \end{aligned} \tag{23}$$

where NE is the total number of elements, and

$$\begin{aligned} \mathbf{C} &= \int_0^{l_e} (\mathbf{c}_w^T \mathbf{c}_w)\mathrm{d}x = \frac{2}{l_e^3}\begin{bmatrix} 6 & 3l_e & -6 & 3l_e \\ 3l_e & 2l_e^2 & -3l_e & l_e^2 \\ -6 & -3l_e & 6 & -3l_e \\ 3l_e & l_e^2 & -3l_e & 2l_e^2 \end{bmatrix}, \\ \mathbf{H} &= \int_0^{l_e} (\mathbf{h}^T \mathbf{h})\mathrm{d}x = \frac{l_e}{6}\begin{bmatrix} 2 & 1 \\ 1 & 2 \end{bmatrix}, \quad \mathbf{c} = \int_0^{l_e} \mathbf{c}_w \mathrm{d}x = \{0,\ -1,\ 0,\ 1\}. \end{aligned} \tag{24}$$

The work of external forces in Eq. (12) can be rewritten as

$$\mathcal{W}_{ex} = \sum^{\mathrm{NE}} \mathcal{W}_{ex}^e = \sum^{\mathrm{NE}} \Big(\int_0^{l_e} (\mathbf{h}_w \boldsymbol{w}_0) q(x)\mathrm{d}x \ + \ \sum_{i=1}^{n_Q^e} Q_i^e (\mathbf{h}_w|_{x=x(Q_i^e)} \boldsymbol{w}_0)\Big), \tag{25}$$

where n_Q^e is the number of concentrated loads acting on the considering beam element.

The internal force vector $\mathbf{f}_{in}^e$ is obtained by differentiating the strain energy (23) with respect to the nodal displacements as

$$\underset{(8\times 1)}{\mathbf{f}_{in}^e} = \frac{\partial \mathcal{U}^e}{\partial \boldsymbol{\Delta}_e} = \{\mathbf{f}_{in}^u,\ \mathbf{f}_{in}^w,\ \mathbf{f}_{in}^\gamma\}^T, \tag{26}$$

where

$$\underset{(2\times 1)}{\mathbf{f}_{in}^u} = \frac{\partial \mathcal{U}^e}{\partial \boldsymbol{u}_0} = EA\, l_e \Big((\mathbf{b}^T \mathbf{b})\boldsymbol{u}_0 + \mathbf{b}^T(\boldsymbol{w}_0^T \mathbf{B})\, \boldsymbol{w}_0\Big), \tag{27}$$

$$\begin{aligned} \underset{(4\times 1)}{\mathbf{f}_{in}^w} = \frac{\partial \mathcal{U}^e}{\partial \boldsymbol{w}_0} &= 2EA\, l_e \Big(\mathbf{b}\boldsymbol{u}_0 + \boldsymbol{w}_0^T \mathbf{B}\, \boldsymbol{w}_0\Big)(\mathbf{B}\, \boldsymbol{w}_0) \\ &\quad + EI\Big[\mathbf{C}\, \boldsymbol{w}_0 - \frac{4}{5}(\mathbf{c}^T \mathbf{b})\, \boldsymbol{\gamma}_0\Big] + GA\ell^2\Big[\mathbf{C}\, \boldsymbol{w}_0 - \frac{1}{3}(\mathbf{c}^T \mathbf{b})\, \boldsymbol{\gamma}_0\Big], \end{aligned} \tag{28}$$

$$\begin{aligned}\underset{(2\times1)}{\mathbf{f}_{in}^{\gamma}} &= \frac{\partial \mathcal{U}^e}{\partial \boldsymbol{\gamma}_0} = \frac{8}{15}GA\mathbf{H}\boldsymbol{\gamma}_0 + EI\Big[\frac{68\,l_e}{105}(\mathbf{b}^T\mathbf{b})\,\boldsymbol{\gamma}_0 - \frac{4}{5}(\mathbf{b}^T\mathbf{c}_w)\boldsymbol{w}_0\Big] \\ &\quad + GA\ell^2\Big[\frac{2}{15}(\mathbf{b}^T\mathbf{b})\boldsymbol{\gamma} - \frac{1}{3}(\mathbf{b}^T\mathbf{c}_w)\boldsymbol{w}_0 + \frac{4}{3h^2}(\mathbf{h}^T\mathbf{h})\boldsymbol{\gamma}\Big].\end{aligned} \tag{29}$$

The element vector of external forces, $\mathbf{f}_{ex}^e$, can also be written in a matrix form as

$$\underset{(8\times1)}{\mathbf{f}_{ex}^e} = \frac{\partial \mathcal{W}_{ex}^e}{\partial \boldsymbol{\Delta}_e} = \left\{\mathbf{0},\ \int_0^{l_e} q(x)\mathbf{h}_w^T \mathrm{d}x + \sum^{n_Q^e}\mathbf{h}_w^T|_{x(Q_i^e)},\ \mathbf{0}\right\}^T. \tag{30}$$

By assembling the derived element vectors $\mathbf{f}_{in}^e$ and $\mathbf{f}_{ex}^e$ over the total number of elements, one can construct equilibrium equation in the following form [21]

$$\mathbf{R}(\mathbf{D},\ \mathbf{F}_{ex}) = \mathbf{F}_{ex} - \mathbf{F}_{in}(\mathbf{D}) = 0, \tag{31}$$

with $\mathbf{D}$ is the global vector of degrees of freedom, $\mathbf{F}_{ex}$, $\mathbf{F}_{in}$, and $\mathbf{R}$ are the global vectors of the external force, internal force and the residual force.

The global tangent stiffness matrix is obtained by incremental change of the global internal force as

$$\mathbf{K}_t(\mathbf{D}) = \frac{\partial \mathbf{F}_{in}(\mathbf{D})}{\partial \mathbf{D}}. \tag{32}$$

This matrix is obtained by assembling the element tangent stiffness matrices over the elements, which are defined as

$$\underset{(8\times8)}{\mathbf{k}_t^e} = \frac{\partial \mathbf{f}_{in}^e}{\partial \boldsymbol{\Delta}_e} = \begin{bmatrix} \mathbf{k}_t^{uu} & \mathbf{k}_t^{uw} & \mathbf{0} \\ (\mathbf{k}_t^{uw})^T & \mathbf{k}_t^{ww} & \mathbf{k}_t^{w\gamma} \\ \mathbf{0} & (\mathbf{k}_t^{w\gamma})^T & \mathbf{k}_t^{\gamma\gamma} \end{bmatrix}. \tag{33}$$

The sub-matrices in the above equation have the following forms

$$\begin{aligned}
\underset{(2\times2)}{\mathbf{k}_t^{uu}} &= \frac{\partial \mathbf{f}_{in}^u}{\partial \boldsymbol{u}_0} = EAl_e(\mathbf{b}^T\mathbf{b}), \quad \underset{(2\times4)}{\mathbf{k}_t^{uw}} = \frac{\partial \mathbf{f}_{in}^u}{\partial \boldsymbol{w}_0} = 2EA\,l_e\mathbf{b}_w^T(\boldsymbol{w}_0^T\mathbf{B}), \\
\underset{(4\times4)}{\mathbf{k}_t^{ww}} &= \frac{\partial \mathbf{f}_{in}^w}{\partial \boldsymbol{w}_0} = EA\,l_e\left\{6(\mathbf{B}\boldsymbol{w}_0)(\boldsymbol{w}_0^T\mathbf{B}) + 2(\mathbf{b}\boldsymbol{u}_0)\mathbf{B}\right\} + (EI + GA\ell^2)\mathbf{C}, \\
\underset{(4\times2)}{\mathbf{k}_t^{w\gamma}} &= \frac{\partial \mathbf{f}_{in}^w}{\partial \boldsymbol{\gamma}_0} = -\left\{\frac{4}{5}EI + \frac{1}{3}GA\ell^2\right\}(\mathbf{c}^T\mathbf{b}), \\
\underset{(2\times2)}{\mathbf{k}_t^{\gamma\gamma}} &= \frac{\partial \mathbf{f}_{in}^{\gamma}}{\partial \boldsymbol{\gamma}_0} = GA\Big(\frac{8}{15} + \frac{4\ell^2}{3h^2}\Big)\mathbf{H} + \left\{\frac{68}{105}EI + \frac{2}{15}GA\ell^2\right\}l_e(\mathbf{b}^T\mathbf{b}).
\end{aligned} \tag{34}$$

The global tangent stiffness is now used in the following linearized equilibrium equation

$$\mathbf{K}_t(\mathbf{D})\delta\mathbf{D} = \mathbf{R}(\mathbf{D}, \mathbf{F}_{ex}) = \mathbf{F}_{ex} - \mathbf{F}_{in}(\mathbf{D}). \tag{35}$$

The above nonlinear equation can be solved for the global vector of degrees of freedom $\mathbf{D}$ by the Newton–Raphson iterative method. The details of the method and its implementation are given in [21,22].

A convergence criterion is needed for the iterative procedure. In the present work, an Euclidean norm based criterion is employed as

$$\|\mathbf{R}\| \leq \varepsilon \|\mathbf{F}_{ex}\|, \tag{36}$$

with ε is the tolerance, which is chosen by 10^{-4} herein.

4. NUMERICAL INVESTIGATION

Table 1. Material and geometric data for microbeams

Geometric data			Material data	
Length L (μm)	Width b (μm)	Thickness h (μm)	Young's modulus E (MPa)	Poisson's ratio ν
250	50	3	169	0.06

Various silicon microbeams as depicted in Fig. 1 with the material data listed in Table 1 [1] are employed in numerical investigation in this section. Three types of applied loads, namely uniformly distributed loads, triangular distributed load, and concentrated load as shown in Fig. 1 are considered. The essential boundary conditions of the microbeams in Fig. 1 are as follows:

(a) Clamped – clamped (CC):

$$u_0(0) = w_0(0) = w_{0,x}(0) = \gamma_0(0) = u_0(L) = w_0(L) = w_{0,x}(L) = \gamma_0(L) = 0. \tag{37}$$

(b) Clamped–pinned (CP):

$$u_0(0) = w_0(0) = w_{0,x}(0) = \gamma_0(0) = u_0(L) = w_0(L) = 0. \tag{38}$$

(c) Pinned–pinned (PP):

$$u_0(0) = w_0(0) = u_0(L) = w_0(L) = 0. \tag{39}$$

(d) Simply supported (SS):

$$u_0(0) = w_0(0) = w_0(L) = 0. \tag{40}$$

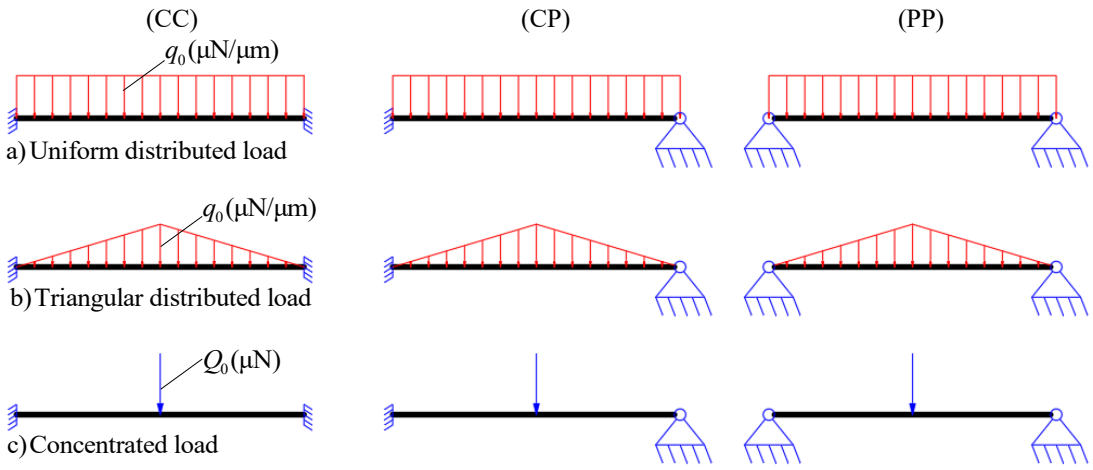

Fig. 1. Considered microbeam models and applied loads (q_0 = 10 μN/μm, Q_0 = 500 μN)

4.1. Formulation verification

The derived beam element is validated herein by comparing the obtained result with available data. In Table 2, the maximum deflections of a macrobeam with CC and PP end conditions under a uniform load $q_0 = 10$ (lb/in) obtained by the present formulation are compared with the results of Refs. [22, 23]. The deflections in Table 2 are determined by the present formulation by setting $\ell^* = 0$ (without the microstructural size effect). The material and geometric data for the microbeam are as follows: $E = 30$ (Msi), $\nu = 0.25$, $L = 100$ (in), $b = h = 1$ (in). Good agreement between the maximum deflections of the present work with the result of [22, 23] can be seen from Table 2, regardless of the boundary conditions and the loading intensity q_0. The error in Table 2 is defined as follows

$$\begin{aligned} \text{Er}_1 &= \frac{|\text{Present result - Ref. [22]}|}{\text{Ref. [22]}} \times 100\%, \\ \text{Er}_2 &= \frac{|\text{Present result - Ref. [23]}|}{\text{Ref. [23]}} \times 100\%. \end{aligned} \tag{41}$$

It is necessary to mention that the load step and the number of load increments used for Table 2 are d$q_0 = 1$ (lb/in) and nINC = 10, respectively.

To verify the beam element in modeling the nonlinear response of microbeams, the accuracy and convergence of the derived beam element in evaluating the dimensionless central deflections of a simply microbeam subjected to uniformly distributed load are shown in Table 3. The data used to obtain the results in the table are E = 1.44 GPa, ν = 0.38, $h = 5 \times 17.6$ μm, $b = 2h$, $L = 20h$, $q_0 = 1$ (N/m) as in Refs. [13, 24]. For

comparison, the results obtained by the shooting method of Ref. [13] and the analytical method of Ref. [24] are also given in Table 3. The Euler–Bernoulli beam theory is used in Ref. [13], while both the Euler–Bernoulli and Timoshenko beam theories are employed in Ref. [24]. Table 3 shows a good agreement between the result of the present work with the cited references, especially with the Timoshenko beam model of Ref. [24]. Table 3 also shows the fast convergence of the present beam element, and the nonlinear response of the microbeam can be accurately predicted by using only four elements.

Table 2. Comparison of maximum deflections of macrobeam under uniformly distributed load

q_0	PP					CC				
	[22]	[23]	Present	Er_1	Er_2	[22]	[23]	Present	Er_1	Er_2
1	0.3685	0.3693	0.3703	0.4885	0.2708	0.1034	0.1035	0.1034	0.0000	0.0966
2	0.5454	0.5467	0.5491	0.6784	0.4390	0.2025	0.2025	0.2024	0.0494	0.0494
3	0.6640	0.6655	0.6690	0.7530	0.5259	0.2943	0.2943	0.2942	0.0340	0.0340
4	0.7555	0.7536	0.7616	0.8074	1.0616	0.3779	0.3777	0.3778	0.0265	0.0265
5	0.8312	0.8316	0.8382	0.8422	0.7937	0.4537	0.4534	0.4536	0.0220	0.0441
6	0.8964	0.8993	0.9041	0.8590	0.5337	0.5224	0.5220	0.5224	0.0000	0.0766
7	0.9540	0.9588	0.9623	0.8700	0.3650	0.5850	0.5845	0.5850	0.0000	0.0855
8	1.0058	1.0205	1.0147	0.8849	0.5683	0.6424	0.6418	0.6424	0.0000	0.0935
9	1.0531	1.0525	1.0626	0.9021	0.9596	0.6954	0.6946	0.6954	0.0000	0.1152
10	1.0967	1.1139	1.1067	0.9118	0.6464	0.7445	0.7436	0.7445	0.0000	0.1210

Table 3. Accuracy and convergence of the beam element in evaluating the dimensionless central deflections of simply microbeam subjected to uniformly distributed load

ℓ^*	Present			Source		
	NE = 2	NE = 4	NE = 6	Ref. [13]	Ref. [24]^a	Ref. [24]^b
0	1.3107	1.3107	1.3107	1.2667	1.3021	1.3103
0.2	1.1162	1.1162	1.1162	1.0900	1.1092	1.1162
0.4	0.7724	0.7724	0.7724	0.7633	0.7679	0.7731
0.6	0.5105	0.5105	0.5105	0.5067	0.5076	0.5116
0.8	0.3462	0.3462	0.3462	0.3440	0.3442	0.3475
1	0.2449	0.2449	0.2449	0.2434	0.2435	0.2464

Note: ^{a}: Based on Euler-Bernoulli beam theory, ^{b}: Based on Timoshenko beam theory.

4.2. Numerical results

For the sake of discussion, the dimensionless parameters for the material length scale parameter, mid-span bending moment and maximum deflection are introduced

as [1,22,23]

$$\ell^* = \frac{\ell}{h}, \quad w^* = 100\frac{EI}{L^4}\, w_0^{\max}, \quad M^* = -\frac{EI}{q_0 b^2}\, w_{0,xx}\Big(\frac{L}{2}\Big), \tag{42}$$

where $w_0^{\max}$ is the maximum deflection.

Table 4. The dimensionless maximum deflections of microbeams under uniformly distributed load

B.C.	q_0	ℓ^*								
		0.1	0.2	0.3	0.4	0.5	0.6	0.7	0.8	0.9
CC	1	0.2419	0.2098	0.1714	0.1362	0.1077	0.0857	0.0690	0.0563	0.0466
	2	0.4615	0.4062	0.3365	0.2698	0.2143	0.1709	0.1378	0.1126	0.0932
	3	0.6512	0.5826	0.4911	0.3987	0.3189	0.2553	0.2062	0.1687	0.1397
	4	0.8137	0.7385	0.6333	0.5215	0.4209	0.3386	0.2742	0.2245	0.1861
	5	0.9545	0.8764	0.7632	0.6374	0.5195	0.4204	0.3415	0.2801	0.2324
	6	1.0782	0.9993	0.8818	0.7463	0.6145	0.5004	0.4080	0.3353	0.2785
	7	1.1886	1.1099	0.9904	0.8484	0.7057	0.5786	0.4736	0.3900	0.3243
	8	1.2883	1.2104	1.0903	0.9441	0.7929	0.6546	0.5381	0.4443	0.3700
	9	1.3794	1.3026	1.1827	1.0340	0.8764	0.7286	0.6016	0.4980	0.4153
	10	1.4633	1.3877	1.2686	1.1185	0.9561	0.8003	0.6639	0.5511	0.4604
CP	1	0.4371	0.3904	0.3285	0.2664	0.2129	0.1704	0.1376	0.1125	0.0932
	2	0.7289	0.6739	0.5928	0.5002	0.4110	0.3343	0.2723	0.2237	0.1858
	3	0.9370	0.8825	0.7984	0.6955	0.5876	0.4875	0.4020	0.3325	0.2772
	4	1.1001	1.0474	0.9646	0.8593	0.7429	0.6282	0.5250	0.4379	0.3669
	5	1.2356	1.1849	1.1042	0.9995	0.8798	0.7567	0.6409	0.5394	0.4545
	6	1.3526	1.3036	1.2252	1.1221	1.0017	0.8739	0.7494	0.6366	0.5397
	7	1.4560	1.4086	1.3323	1.2312	1.1113	0.9813	0.8509	0.7294	0.6224
	8	1.5491	1.5030	1.4287	1.3296	1.2110	1.0801	0.9460	0.8178	0.7023
	9	1.6341	1.5892	1.5166	1.4196	1.3025	1.1716	1.0352	0.9020	0.7795
	10	1.7124	1.6686	1.5977	1.5025	1.3870	1.2567	1.1190	0.9821	0.8539
PP	1	0.7266	0.6897	0.6312	0.5573	0.4769	0.3996	0.3317	0.2755	0.2302
	2	1.0275	0.9964	0.9452	0.8759	0.7923	0.7004	0.6077	0.5210	0.4446
	3	1.2287	1.2015	1.1561	1.0933	1.0149	0.9245	0.8271	0.7289	0.6358
	4	1.3847	1.3602	1.3189	1.2612	1.1881	1.1018	1.0057	0.9046	0.8038
	5	1.5142	1.4917	1.4536	1.4000	1.3314	1.2492	1.1560	1.0554	0.9517
	6	1.6258	1.6049	1.5694	1.5191	1.4542	1.3759	1.2859	1.1871	1.0831
	7	1.7247	1.7051	1.6717	1.6241	1.5624	1.4875	1.4007	1.3042	1.2011
	8	1.8138	1.7953	1.7637	1.7185	1.6596	1.5876	1.5038	1.4097	1.3081
	9	1.8952	1.8777	1.8477	1.8045	1.7480	1.6787	1.5975	1.5059	1.4061
	10	1.9704	1.9538	1.9251	1.8837	1.8293	1.7624	1.6837	1.5945	1.4965

The dimensionless maximum deflections of the CC, CP, PP microbeam under a uniform distributed load are given in Table 4 for various values of scale parameter ℓ^*. It is evident from the table that the material length scale parameter has a significant impact on the maximum nonlinear deflections of the microbeams. For all the considered boundary conditions, the deflections are lower for the microbeams associated with higher scale parameter ℓ^*, regardless of load level. Thus, the material length scale which has been taken into consideration herein make the microbeam stiffer, and the deflection is overestimated when ignore the microstructral size effect.

The results for the dimensionless maximum nonlinear deflections of the microbeams under the triangular distributed load (Fig. 1(b)) and a concentrated load (Fig. 1(c)) are given in Tables 5 and 6, respectively. As expected, the maximum nonlinear deflection of the microbeam under the triangular distributed load is smaller than that compared to the one under the uniformly distributed load, regardless of the scale parameter and the loading level as well.

Table 5. The dimensionless maximum deflections of microbeams under triangular distributed load

B.C.	q_0	ℓ^*								
		0.1	0.2	0.3	0.4	0.5	0.6	0.7	0.8	0.9
CC	1	0.1709	0.1477	0.1204	0.0955	0.0754	0.0600	0.0483	0.0394	0.0326
	2	0.3332	0.2905	0.2385	0.1901	0.1505	0.1198	0.0965	0.0788	0.0653
	3	0.4818	0.4248	0.3525	0.2830	0.2249	0.1794	0.1447	0.1182	0.0979
	4	0.6156	0.5490	0.4611	0.3734	0.2982	0.2385	0.1926	0.1575	0.1304
	5	0.7355	0.6630	0.5638	0.4609	0.3703	0.2971	0.2403	0.1966	0.1629
	6	0.8434	0.7674	0.6602	0.5452	0.4409	0.3551	0.2877	0.2357	0.1954
	7	0.9412	0.8633	0.7507	0.6261	0.5098	0.4123	0.3348	0.2745	0.2278
	8	1.0305	0.9517	0.8356	0.7036	0.5770	0.4686	0.3815	0.3132	0.2601
	9	1.1126	1.0336	0.9153	0.7776	0.6423	0.5241	0.4278	0.3517	0.2923
	10	1.1886	1.1099	0.9904	0.8484	0.7057	0.5786	0.4736	0.3900	0.3243
CP	1	0.3077	0.2703	0.2236	0.1790	0.1421	0.1133	0.0913	0.0746	0.0618
	2	0.5472	0.4950	0.4228	0.3471	0.2796	0.2247	0.1813	0.1488	0.1234
	3	0.7299	0.6740	0.5918	0.4986	0.4092	0.3325	0.2689	0.2224	0.1846
	4	0.8766	0.8204	0.7350	0.6331	0.5294	0.4357	0.3535	0.2948	0.2454
	5	0.9996	0.9442	0.8584	0.7526	0.6400	0.5336	0.4345	0.3660	0.3055
	6	1.1061	1.0518	0.9668	0.8595	0.7416	0.6261	0.5116	0.4357	0.3648
	7	1.2004	1.1473	1.0635	0.9561	0.8353	0.7132	0.5849	0.5036	0.4232
	8	1.2854	1.2334	1.1509	1.0441	0.9218	0.7953	0.6545	0.5697	0.4807
	9	1.3630	1.3120	1.2309	1.1250	1.0022	0.8727	0.7206	0.6340	0.5371
	10	1.4346	1.3846	1.3047	1.2000	1.0772	0.9457	0.7835	0.6963	0.5923

B.C.	q_0	ℓ^*								
		0.1	0.2	0.3	0.4	0.5	0.6	0.7	0.8	0.9
PP	1	0.5604	0.5212	0.4624	0.3935	0.3255	0.2659	0.2172	0.1786	0.1485
	2	0.8315	0.7958	0.7384	0.6640	0.5796	0.4942	0.4157	0.3481	0.2924
	3	1.0140	0.9816	0.9287	0.8578	0.7730	0.6807	0.5885	0.5032	0.4284
	4	1.1554	1.1254	1.0763	1.0094	0.9274	0.8348	0.7376	0.6425	0.5550
	5	1.2726	1.2445	1.1983	1.1349	1.0563	0.9655	0.8673	0.7674	0.6718
	6	1.3737	1.3472	1.3033	1.2429	1.1674	1.0790	0.9815	0.8798	0.7792
	7	1.4632	1.4379	1.3960	1.3382	1.2654	1.1796	1.0836	0.9815	0.8783
	8	1.5439	1.5196	1.4794	1.4237	1.3534	1.2701	1.1759	1.0744	0.9698
	9	1.6177	1.5942	1.5554	1.5016	1.4336	1.3525	1.2603	1.1598	1.0548
	10	1.6858	1.6631	1.6255	1.5734	1.5073	1.4284	1.3380	1.2388	1.1341

Table 6. The dimensionless maximum deflections of microbeams under concentrated load

B.C.	Q_0	ℓ^*								
		0.1	0.2	0.3	0.4	0.5	0.6	0.7	0.8	0.9
CC	50	0.0983	0.0848	0.0689	0.0546	0.0431	0.0343	0.0276	0.0225	0.0187
	100	0.1948	0.1686	0.1374	0.1091	0.0862	0.0685	0.0552	0.0451	0.0373
	150	0.2881	0.2505	0.2051	0.1632	0.1291	0.1028	0.0828	0.0676	0.0559
	200	0.3772	0.3299	0.2716	0.2168	0.1718	0.1369	0.1103	0.0901	0.0746
	250	0.4615	0.4062	0.3365	0.2698	0.2143	0.1709	0.1378	0.1126	0.0932
	300	0.5409	0.4793	0.3998	0.3221	0.2564	0.2048	0.1652	0.1350	0.1118
	350	0.6156	0.5490	0.4611	0.3734	0.2982	0.2385	0.1926	0.1575	0.1304
	400	0.6857	0.6153	0.5205	0.4238	0.3396	0.2721	0.2199	0.1798	0.1490
	450	0.7516	0.6784	0.5779	0.4732	0.3805	0.3054	0.2471	0.2022	0.1676
	500	0.8137	0.7385	0.6333	0.5215	0.4209	0.3386	0.2742	0.2245	0.1861
CP	50	0.1695	0.1470	0.1200	0.0954	0.0754	0.0600	0.0483	0.0394	0.0326
	100	0.3239	0.2849	0.2358	0.1890	0.1501	0.1197	0.0965	0.0788	0.0653
	150	0.4579	0.4091	0.3445	0.2795	0.2234	0.1788	0.1444	0.1181	0.0978
	200	0.5734	0.5195	0.4447	0.3657	0.2949	0.2372	0.1920	0.1572	0.1303
	250	0.6740	0.6176	0.5366	0.4473	0.3642	0.2945	0.2392	0.1961	0.1627
	300	0.7630	0.7054	0.6207	0.5242	0.4310	0.3507	0.2858	0.2348	0.1950
	350	0.8427	0.7848	0.6981	0.5964	0.4952	0.4056	0.3318	0.2732	0.2272
	400	0.9150	0.8572	0.7694	0.6643	0.5568	0.4591	0.3771	0.3112	0.2591
	450	0.9813	0.9238	0.8357	0.7282	0.6157	0.5111	0.4217	0.3489	0.2909
	500	1.0427	0.9856	0.8974	0.7885	0.6721	0.5617	0.4655	0.3862	0.3225

B.C.	Q_0	ℓ^*								
		0.1	0.2	0.3	0.4	0.5	0.6	0.7	0.8	0.9
PP	50	0.3430	0.3078	0.2603	0.2120	0.1698	0.1361	0.1100	0.0899	0.0745
	100	0.5626	0.5229	0.4634	0.3941	0.3258	0.2660	0.2172	0.1787	0.1485
	150	0.7168	0.6783	0.6181	0.5430	0.4625	0.3860	0.3197	0.2650	0.2213
	200	0.8371	0.8003	0.7418	0.6662	0.5809	0.4950	0.4160	0.3483	0.2925
	250	0.9369	0.9017	0.8452	0.7708	0.6843	0.5933	0.5059	0.4279	0.3617
	300	1.0228	0.9890	0.9344	0.8618	0.7756	0.6823	0.5895	0.5037	0.4287
	350	1.0988	1.0662	1.0133	0.9426	0.8574	0.7633	0.6671	0.5755	0.4934
	400	1.1673	1.1356	1.0843	1.0153	0.9315	0.8375	0.7393	0.6435	0.5556
	450	1.2297	1.1989	1.1490	1.0816	0.9993	0.9059	0.8067	0.7080	0.6153
	500	1.2874	1.2573	1.2086	1.1427	1.0619	0.9694	0.8698	0.7690	0.6727

In order to show the effects of the boundary conditions on nonlinear response of the microbeams under the mechanical loading, the load-dimensionless maximum deflection curves of the CC, CP and PP microbeams are shown in Figs. 2–4 for the uniformly distributed load, triangular distributed load, and concentrated load, respectively. One can see from the figures that the boundary conditions play an important role on the nonlinear response of the microbeam. Not only the deflection amplitude by the degree of the nonlinearity also are governed by the boundary conditions. At a given load, both the nonlinear deflection and the nonlinear degree of the SS microbeam is the largest, while the opposite is for the CC microbeam, regardless of the loading type. This tendency is the most clear for the microbeam under the concentrated load (Fig. 4).

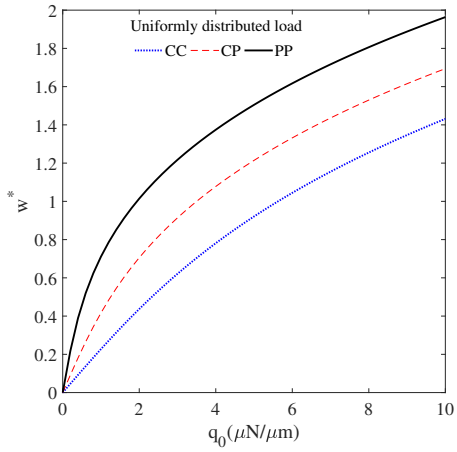

Fig. 2. Load-dimensionless maximum deflection curves of microbeams under uniformly distributed load with $\ell^* = 0.15$

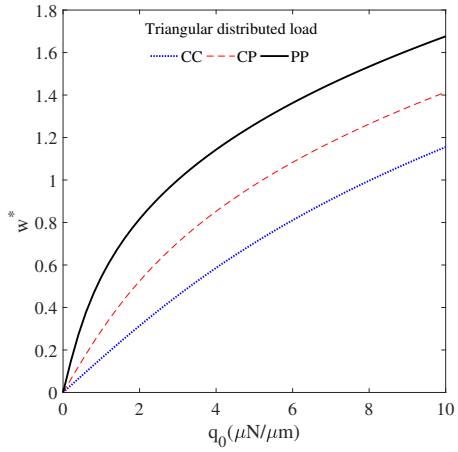

Fig. 3. Load-dimensionless maximum deflection curves of microbeams under triangular distributed load with $\ell^* = 0.25$

To illustrate the influence of the material length scale parameter on the nonlinear bending of the microbeams in more detail, the dimensionless maximum deflection-load curves of the PP and CP microbeams under the uniformed distributed load and concentrated load are respectively shown in Figs. 5 and 6 for various values of the scale parameter ℓ^*. Regardless of the loading level and loading type, the nonlinear deflection of the microbeams is sharply decreased by the increase of the material length scale parameter. This due to the fact the the size effect, which has been taken into account herein, enhances the strain energy, and also the bending and shear stiffness of the microbeams, as can be evident from Eqs. (11) and (34). Thus, the microstructral effect has important influence on predicting nonlinear response of the microbeams, and the deflections are considerably overestimated when ignore the micro-size effect.

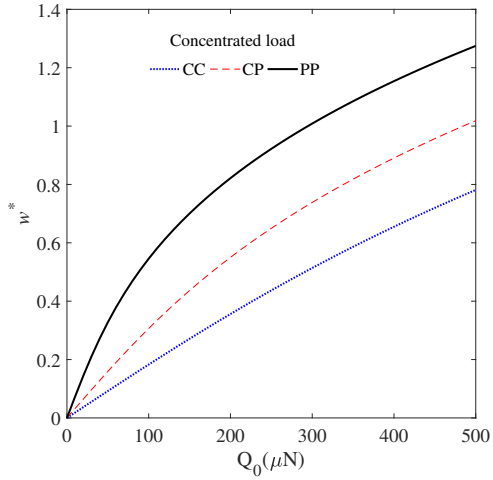

Fig. 4. Load-dimensionless maximum deflection curves of microbeams under concentrated load with $\ell^* = 0.35$

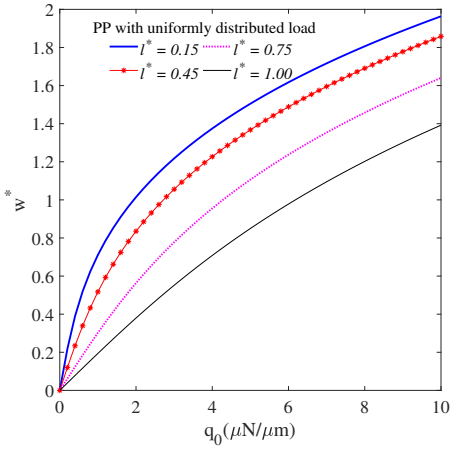

Fig. 5. Load-dimensionless maximum deflection curves of PP microbeams under uniformly distributed load with various values of ℓ^*

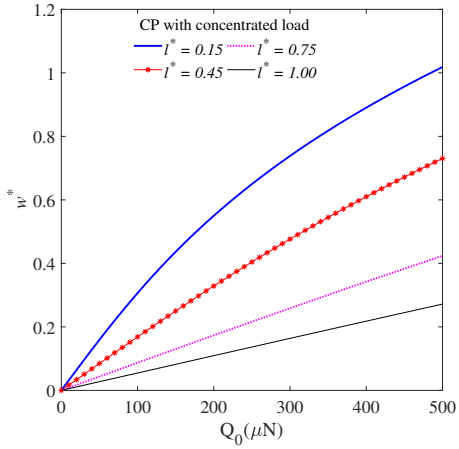

Fig. 6. Load-dimensionless maximum deflection curves of CP microbeams under concentrated load with various values of ℓ^*

Finally, the applied load versus the moment at mid-span section of CC microbeam according to various scale parameters are shown in Figs. 7 and 8 for two cases of applied load, the uniformly distributed load and the triangular distributed load, respectively.

The effect of the microstructural effect on the moment is similar to that of the maximum deflection, and the moment at is decreased with the increasing of the scale parameter. The figures also show the significant influence of the loading type on the moment, and the moment obtained from the uniformly distributed load is higher than that of the triangular distributed load, regardless of the material length scale parameter.

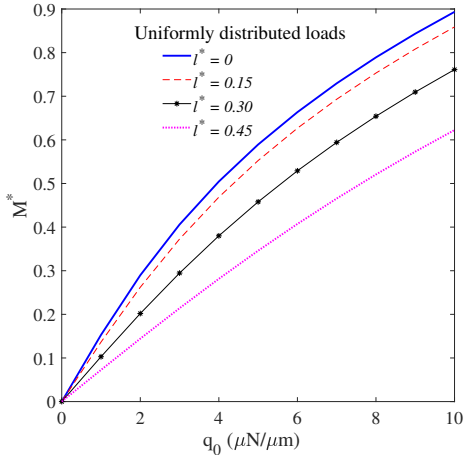

Fig. 7. Applied load versus mid-span moment of CC microbeams under uniformly distributed load with various values of ℓ^*.

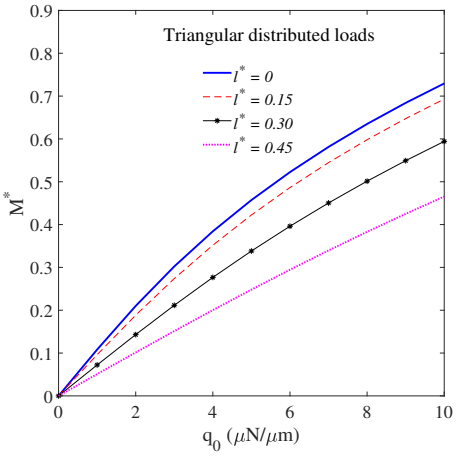

Fig. 8. Applied load versus mid-span moment of CC microbeams under triangular distributed load with various values of ℓ^*.

5. CONCLUSION

The size-dependent nonlinear bending of microbeams under mechanical loading was studied in the present work on the basis of the third-order shear deformation theory. The influence of microstructural size effect on the nonlinear response was captured using the MCST. Based on the von Kármán nonlinear assumption, a nonlinear finite beam element was derived by using the shear rotation as a variable. Using the derived beam element, the discretized nonlinear equilibrium equation has been constructed and then solved by the Newton-Raphson iterative method. The dimensionless maximum deflections of microbeams subjected to various types of distributed and concentrated loads have been computed for different material length scale parameters. The effects of the microstructural parameter and the boundary conditions on the nonlinear response of the microbeam were investigated in detail. The numerical result reveals that the beam element derived herein is capable to predict accurately nonlinear response of microbeams by small number of elements. It was also shown that the microstructural parameter has an important role in the nonlinear response of the microbeams, and the deflections are considerably overestimated by ignoring the micro-size effect. It is worth noting that the

beam element formulated in the present work can be used to analyze microbeams subjected to other types of loading as well. In addition, the extension of the present work in nonlinear analysis of microframes is straightforward.

DECLARATION OF COMPETING INTEREST

The authors declare that they have no known competing financial interests or personal relationships that could have appeared to influence the work reported in this paper.

ACKNOWLEDGMENT

This article was supported by National Foundation for Science and Technology Development (NAFOSTED) of Vietnam, the Grant 107.02.2021.11.

REFERENCES

[1] M. I. Younis. *MEMS linear and nonlinear statics and dynamics*, Vol. 20. Springer Science & Business Media, (2011).

[2] B. Choi and E. G. Lovell. Improved analysis of microbeams under mechanical and electrostatic loads. *Journal of Micromechanics and Microengineering*, **7**, (1), (1997). https://doi.org/10.1088/0960-1317/7/1/005.

[3] E. M. Abdel-Rahman and A. H. Nayfeh. Secondary resonances of electrically actuated resonant microsensors. *Journal of Micromechanics and Microengineering*, **13**, (3), (2003). https://doi.org/10.1088/0960-1317/13/3/320.

[4] S. Chaterjee and G. Pohit. A large deflection model for the pull-in analysis of electrostatically actuated microcantilever beams. *Journal of Sound and Vibration*, **322**, (4-5), (2009), pp. 969–986. https://doi.org/10.1016/j.jsv.2008.11.046.

[5] D. C. C. Lam, F. Yang, A. C. M. Chong, J. Wang, and P. Tong. Experiments and theory in strain gradient elasticity. *Journal of the Mechanics and Physics of Solids*, **51**, (8), (2003), pp. 1477–1508. https://doi.org/10.1016/s0022-5096(03)00053-x.

[6] M. H. Kahrobaiyan, M. Asghari, M. Rahaeifard, and M. T. Ahmadian. A nonlinear strain gradient beam formulation. *International Journal of Engineering Science*, **49**, (11), (2011), pp. 1256–1267. https://doi.org/10.1016/j.ijengsci.2011.01.006.

[7] F. A. C. M. Yang, A. C. M. Chong, D. C. C. Lam, and P. Tong. Couple stress based strain gradient theory for elasticity. *International Journal of Solids and Structures*, **39**, (10), (2002), pp. 2731–2743. https://doi.org/10.1016/s0020-7683(02)00152-x.

[8] H. Mohammadi and M. Mahzoon. Thermal effects on postbuckling of nonlinear microbeams based on the modified strain gradient theory. *Composite Structures*, **106**, (2013), pp. 764–776. https://doi.org/10.1016/j.compstruct.2013.06.030.

[9] W. Xia, L. Wang, and L. Yin. Nonlinear non-classical microscale beams: static bending, postbuckling and free vibration. *International Journal of Engineering Science*, **48**, (12), (2010), pp. 2044–2053. https://doi.org/10.1016/j.ijengsci.2010.04.010.

[10] M. Asghari, M. H. Kahrobaiyan, and M. T. Ahmadian. A nonlinear Timoshenko beam formulation based on the modified couple stress theory. *International Journal of Engineering Science*, **48**, (12), (2010), pp. 1749–1761. https://doi.org/10.1016/j.ijengsci.2010.09.025.

[11] S. Ramezani. A micro scale geometrically non-linear Timoshenko beam model based on strain gradient elasticity theory. *International Journal of Non-Linear Mechanics*, **47**, (8), (2012), pp. 863–873. https://doi.org/10.1016/j.ijnonlinmec.2012.05.003.

[12] B. Akgöz and Ö. Civalek. Buckling analysis of functionally graded microbeams based on the strain gradient theory. *Acta Mechanica*, **224**, (9), (2013), pp. 2185–2201. https://doi.org/10.1007/s00707-013-0883-5.

[13] Y.-G. Wang, W.-H. Lin, and N. Liu. Nonlinear bending and post-buckling of extensible microscale beams based on modified couple stress theory. *Applied Mathematical Modelling*, **39**, (1), (2015), pp. 117–127. https://doi.org/10.1016/j.apm.2014.05.007.

[14] R. Ansari, M. F. Shojaei, and R. Gholami. Size-dependent nonlinear mechanical behavior of third-order shear deformable functionally graded microbeams using the variational differential quadrature method. *Composite Structures*, **136**, (2016), pp. 669–683. https://doi.org/10.1016/j.compstruct.2015.10.043.

[15] F. Dadgar-Rad and A. Beheshti. A nonlinear strain gradient finite element for microbeams and microframes. *Acta Mechanica*, **228**, (5), (2017), pp. 1941–1964. https://doi.org/10.1007/s00707-017-1798-3.

[16] M. A. Attia and S. A. Mohamed. Nonlinear thermal buckling and postbuckling analysis of bidirectional functionally graded tapered microbeams based on Reddy beam theory. *Engineering with Computers*, (2022), pp. 1–30.

[17] J. N. Reddy. A simple higher-order theory for laminated composite plates. *Journal of Appllied Mechanics*, **54**, (4), (1984), pp. 745–752. https://doi.org/10.1115/1.3167719.

[18] G. Shi and K. Y. Lam. Finite element vibration analysis of composite beams based on higher-order beam theory. *Journal of Sound and Vibration*, **219**, (4), (1999), pp. 707–721. https://doi.org/10.1006/jsvi.1998.1903.

[19] C. I. Le, V. N. Pham, and D. K. Nguyen. Size dependent pull-in instability of functionally graded microbeams using a finite element formulation. In *IOP Conference Series: Materials Science and Engineering*, IOP Publishing, Vol. 1289, (2023). https://doi.org/10.1088/1757-899x/1289/1/012028.

[20] M. A. Crisfield. *Nonlinear finite element analysis of solids and structures. Volume 1: Essentials*. Wiley, New York, (1991).

[21] S. Krenk. *Non-linear modeling and analysis of solids and structures*. Cambridge University Press, (2009). https://doi.org/10.1017/cbo9780511812163.

[22] J. N. Reddy. *An Introduction to Nonlinear Finite Element Analysis: with applications to heat transfer, fluid mechanics, and solid mechanics*. Oxford University Press, (2015).

[23] R. Ranjan. Nonlinear finite element analysis of bending of straight beams using hp-spectral approximations. *Journal of Solid Mechanics*, (2011).

[24] J. N. Reddy. Microstructure-dependent couple stress theories of functionally graded beams. *Journal of the Mechanics and Physics of Solids*, **59**, (11), (2011), pp. 2382–2399. https://doi.org/10.1016/j.jmps.2011.06.008.